An *in-vitro* Study of Wireless Inductive Sensing and Robust Packaging for Future Implantable Hydrogel-based Glucose Monitoring Applications

Yuechuan Yu, Tram Nguyen, Prashant Tathireddy, Shad Roundy, *Member, IEEE*, Darrin J. Young, *Member, IEEE*

Abstract—**A wireless inductive sensing technology with a robust packaging scheme is proposed and demonstrated for future implantable hydrogel-based glucose monitoring applications. A prototype wireless glucose sensor employs a glucose-sensitive hydrogel embedding a parylene-coated metallic sensing plate as a key sensing element. The hydrogel changes its volume responding to glucose change; thus displacing the metallic sensing plate that can be sensed by a nearby sensing coil through the coil inductance change. An ultra-low-power tunnel diode oscillator is designed to convert the inductance change to an oscillator frequency change, which can be wirelessly detected by a nearby receiver. The entire sensing system can be energized by RF powering, thus achieving a wireless and battery-less operation. The proposed sensing scheme allows the sensing electronics to be fully encapsulated in a hermetically sealed package, critical for long-term implantable applications. *In vitro* characterization demonstrates that the prototype sensor operated around 40 MHz can be wirelessly powered by a 2.77 mW 5 MHz power source with a distance of 2 cm, and achieves a sensing resolution of 0.05 mM and 0.3 mM within a glucose range from 0 mM to 2 mM and 8 mM to 10 mM, respectively, limited by the oscillator frequency drift and fluctuation. Furthermore, a hydrogel pillar-based design is promising to substantially shorten the system response time.**

***Index Terms*—Inductive sensing, wireless sensing, glucose monitoring, RF powering, inductive powering, sensor packaging, hydrogel, glucose-sensitive hydrogel, biomedical implant.**

I. Introduction

Diabetes mellitus is a global epidemic that currently affects more than 400 million people worldwide. Self-monitoring of blood glucose is an essential way for management of diabetes and its related complications. Conventionally, such a measurement is performed by using a figure-prick method, which requires a lancing device drawing a small amount of blood sample and a hand-held glucometer. Aside from its inconvenience and poor patient compliance, the main limitation of the finger-prick method is that it only provides a point measurement, which does not carry critical information such as glucose trend and daily peaks. Continuous glucose monitoring (CGM) has been proposed as an attractive alternative to managing diabetes because it can provide a comprehensive blood glucose profile. Such a profile can be used to predict and avoid hypoglycemia as well as hyperglycemia, critical for preventing life-threatening events and alleviating diabetic-related complications. Enzyme-based electrochemical sensors have been widely used in commercial CGM systems. However, these sensors measure glucose from interstitial fluid (ISF) by using a partially implanted needle in the subcutaneous tissue [1]. There are a number of drawbacks associated with this type of CGM. For example, the sensor needs to be frequently calibrated and replaced due to enzyme denaturation, and the partially implanted needle causes an open wound that can increase the chance of infection. In recent years, a significant amount of research effort has been devoted to improving CGMs. Most of the approaches are based on measuring the glucose concentration indirectly from bodily fluid other than blood, such as ISF, tears, saliva, and sweat. Contact lens-based tear glucose sensors have drawn attention due to their non-invasiveness [2]. However, the sensors suffer from a low glucose concentration in tears as well as a low tears sample volume. Furthermore, assessments of blood glucose from tears sample with consistency remains to be a challenge. Saliva and sweat have also been investigated for non-invasive glucose measurement [3, 4], but the former can be sensitive to food residue and the sweat collection can be inconvenient. Other non-invasive approaches use transdermal techniques based on reverse iontophoresis [5] and sonophoresis [6], which extract ISF from underneath the skin. These methods cause skin irritation, and collecting the extracted ISF can be difficult. Optical methods such as near-infrared (NIR) spectroscopy have also been explored to measure glucose concentration [7] with drawbacks including lack of specificity and being sensitive to physiological and environmental variations [8]. Fluorescence-based glucose sensing has gained attention due to its potential for long-term implantable applications [9]. A fluorescent glucose sensor based on hydrogel fiber implanted in

This manuscript is submitted for review on March 7, 2019. This work was supported in part by the U.S. National Science Foundation under Grant ECCS - 1408265.

Yuechuan Yu, Shad Roundy, and Darrin J. Young are with the University of Utah, Salt Lake City, UT 84112 USA (e-mail: darrin.young@utah.edu).

Tram Nguyen, was with the University of Utah, Salt Lake City, UT 84112 USA.

Prashant Tathireddy is with Applied Biosensors, LLC, UT 84115 USA (e-mail: p.tathireddy@appliedbiosensors.com).

a laboratory mouse's ear has been reported. The sensor can measure *in-vivo* glucose concentration for up to 140 days [10]. Two other fluorescent glucose sensors employing a UV LED interfaced with a CMOS chip and photo-detector have been demonstrated with a life time of 90 days *in vivo* and 150 days *in vitro*, respectively [11, 12]. The fluorescent sensors, however, can dissipate excessive power due to the usage of a light source and potentially suffer from photo-bleaching, limiting system sensitivity and lifetime. Furthermore, high power dissipation would call for ferrite-based implantable antennas to achieve a sufficient transcutaneous coupling to enable wireless power transfer and data telemetry. Ferrite, however, renders the implants MRI incompatible. Parallel to the research efforts described above, glucose-sensitive hydrogels (GSH) have been explored for designing glucose sensors. Many *in-vivo* studies on implantable hydrogel-based biomedical systems have shown its excellent biocompatibility; hence, suitable for long-term implantable applications [13, 14]. GSH can change its volume responding to a glucose concentration change. Various methods have been proposed to detect the volume change by employing membrane-based capacitive sensing and pressure sensing principles as well as magnetic-based sensing techniques [15-17]. These approaches exhibit certain drawbacks such as potential membrane and package leakage, and MRI incompatibility. To overcome the limitations aforementioned, we propose an implantable hydrogel-based glucose sensor that can measure glucose from ISF enabled by an inductive sensing scheme, low power wireless telemetry, and robust packaging. Figure 1 depicts the proposed subcutaneous wireless implantable glucose sensing architecture, where radio frequency (RF) wireless powering operated at f_{power} and data telemetry conducted at f_{sense} are employed to enable fully wireless and battery-less operation. An external RF power transmitter can be attached to the skin surface to wirelessly power up the sensor when glucose measurement is needed. The transmitter can be designed as a hand-held device to provide a proactive measurement capability or as a wearable unit enabling an autonomous continuous glucose sensing. This approach can potentially overcome the drawbacks associated with enzymatic sensors and enable a long-term monitoring capability without the need for frequent sensor replacement.

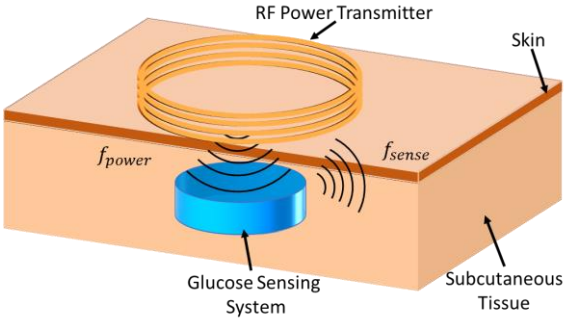

Fig. 1. Subcutaneous wireless implantable glucose sensing architecture.

The proposed sensing architecture employs a glucose-sensitive hydrogel embedding a parylene-coated metallic sensing plate. The hydrogel employed in the prototype design inversely changes its volume responding to an increase in glucose change, thus displacing the embedded metallic sensing plate that can be sensed by a nearby sensing coil through its inductance change (not shown in the figure for simplicity). An ultra-low-power tunnel diode oscillator is then utilized to convert the glucose-induced inductance change to a change in the oscillator frequency, f_{sense}, which can be wirelessly detected by a nearby receiver. The proposed sensing scheme allows the sensing electronics to be fully encapsulated in a hermetically sealed package without any deflectable membrane, which is critical for long-term implantable operations. A prototype sensor was previously implemented, which exhibited some limitations including (1) a long hydrogel response time and (2) an unsatisfactory sensor performance under wireless powering due to supply voltage fluctuation causing frequency instability [18]. This paper presents an improved system design achieving a faster hydrogel response time and a more stable sensor performance under wireless RF powering. To explore the hydrogel characteristics and oscillator-based inductive sensing technique, we demonstrate the key functionalities of a prototype system with a slightly scaled up package and project that the overall system can be miniaturized to mm-scale with electronics implemented in a form of application-specific integrated circuit (ASIC). Section II introduces the overall glucose sensing system design architecture. Section III describes the inductive sensing principle and characterization results. Section IV presents a DC-powered prototype sensing system design, packaging technique, and measurement data. Section V describes an RF-powered glucose sensor with *in-vitro* measurement results. A discussion section focusing on performance comparison is provided in Section VI. Conclusions and future work are given in Section VII.

II. Wireless Implantable Glucose Sensing System

Figure 2 presents a prototype wireless glucose sensing system design architecture, where a circular thin PCB substrate containing the sensing electronics and wireless powering circuitry is placed inside a 10 mm-diameter 3D-printed sensor package (made of VeroClear from Object). The substrate size is limited by the discrete electronic components employed in the current prototype design. A 2 mm-diameter/10-turn spiral sensing coil (made with 45 µm-diameter copper wire) is sandwiched between the PCB substrate and the sensor package bottom plate. The sensor package bottom plate exhibits a thickness of approximately 80 µm. A miniature sensing coil is desirable for future system miniaturization but can be limited by conventional implementation techniques.

The sensor package is then filled with PDMS to seal the electronic components, followed by a 10 µm Parylene C coating serving as a biocompatible and moisture-resistant layer. A 3 mm x 3 mm x 400 µm glucose-sensitive hydrogel embedding a metallic sensing plate on its surface is adhered on a 3D-printed backplate by using Loctite 4011 medical device adhesive. It should be noted that the hydrogel is fabricated on a 200 µm-thick GelBond® film as will be described in Section IV. The size of the hydrogel is selected to be comparable to the dimension of the sensing coil to maximize the sensitivity. The backplate is assembled to the sensor package using three

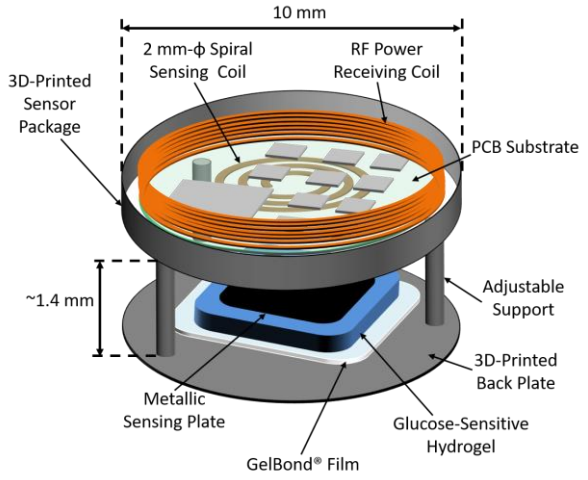

Fig. 2. Packaging scheme of the proposed glucose sensor.

supports with an adjustable length to obtain the desired gap size between the metallic sensing plate and the spiral sensing coil. In the prototype design, three screws (made of nylon or stainless steel) are used to serve as the supports with a height of approximately 1.4 mm while providing adjustability to achieve an initial gap size of approximately 450 µm. A further reduced gap size can result in an increased sensitivity but requiring a careful assembly and a fine adjustment. It should also be noted that a solenoidal coil with a diameter of approximately 10 mm and 20 turns is placed on the PCB substrate to serve as an RF power receiving coil. The solenoidal configuration is selected to minimize the sensor package form factor while achieving an adequate amount of inductance. It is envisioned that a further miniaturized implantable glucose sensing system, employing low-power integrated electronics in an ASIC form, can be realized with a dimension on the order of a few millimeters. The miniaturized system can be potentially incorporated as a part of a blood vessel stent and implanted through a minimally-invasive angioplasty surgery via a catheter [19, 20], thus directly sensing blood glucose, which is planned as a future research step.

Figure 3 illustrates the essential electrical building blocks required to implement the proposed wireless glucose sensing system. The system contains two major functional subsystems: (1) an ultra-low-power tunnel diode oscillator-based glucose sensor that can sense and wirelessly transmit the blood glucose level, and (2) an RF power receiving and conditioning circuity, which is composed of a tuned LC tank as an RF power receiver, a rectifier, and a voltage regulator to deliver a stable DC bias voltage for the oscillator.

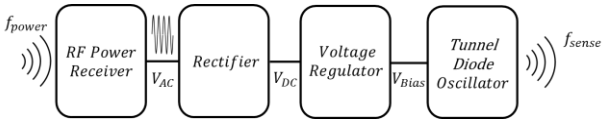

Fig. 3. Block diagram of the proposed wireless glucose sensing system.

The proposed glucose sensor employs an inductive sensing technique that converts a glucose change to the sensing coil inductance change, which in turn modulates the oscillation frequency (f_{sense}) that can be detected by a nearby receiver. The glucose-to-frequency modulation scheme is attractive for achieving a reliable data transmission compared to amplitude modulation techniques.

III. Inductive Sensing Principle and Characterization

A. Inductive Sensing Principle and Characterization

The inductive sensing scheme is based on placing a sensing coil inductor in proximity to a conductive object such as a metallic sensing plate. The alternating magnetic field generated by the coil inductor under an AC excitation induces an eddy current in the metallic sensing plate, which in turn generates a counteracting magnetic field that opposes the coil inductor's magnetic field, thus reducing the inductance value of the sensing coil inductor. As the distance between the sensing coil and the metallic sensing plate changes, the counteracting field-effect also changes, thus resulting in a change of inductance as a function of displacement.

Figure 4(a) shows the test setup for an inductive sensing characterization, where a 3 mm x 3 mm metallic sensing plate is placed in proximity of a 2 mm-diameter/10-turn sensing coil. The gap size between the sensing coil and the metallic sensing plate is controlled by a linear motor stage with an approximately 1 µm displacement resolution. The actual displacement is measured by using an optical displacement sensor (Keyence LK-030). The characterization procedure is described as the following: (1) align the center of the coil with the center of the metallic sensing plate with an initial gap size on the order of a few mm; (2) reduce the initial gap by controlling the linear motor stage until the sensing coil and the metallic sensing plate touch; and (3) increase the gap size and measure the inductance value as a function of gap size.

A more rigorous inductive sensing characterization setup resembling an *in vitro* packaged glucose testing environment is depicted in Figure 4(b). A 3D-printed sensor package is positioned upside down at the bottom of a characterization container to obtain open access of a metallic sensing plate as shown in the figure. The metallic sensing plate is attached to a suspension arm and is controlled by a motor stage as described previously (not depicted in the figure for simplicity). The sensing coil is placed at the bottom of the 3D-printed package and sealed by a PDMS layer. The container is then filled with 1xPBS solution to immerse the sensor package and the metallic sensing plate, emulating an *in vivo* physiological environment.

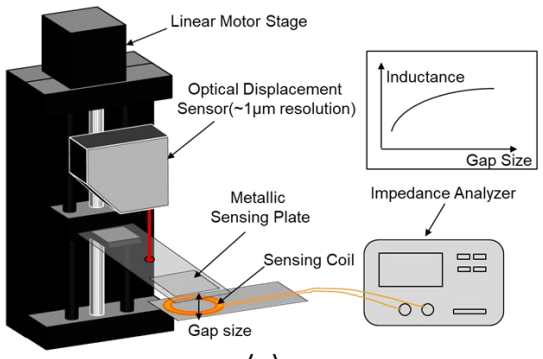

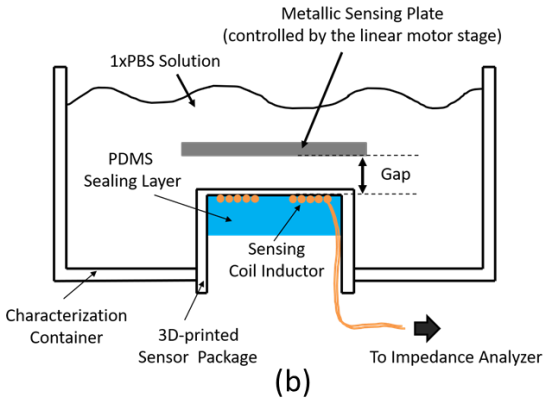

Fig. 4 Inductive sensing characterization.

The characterization starts with an initial gap size of approximately 200 µm (including ~80 µm thickness for the package bottom plate) between the metallic sensing plate and the sensing coil.

The inductance value is then measured with the gap size varying from 200 µm to 900 µm. The measurement result is shown in Figure 5, from which one can make the following observations: (1) within a vicinity of approximately 50 µm at different gap sizes, the inductance exhibits a nearly linear behavior as a function of the gap; and (2) the sensitivity decreases as the gap size increases. To quantify the above observations, a sensitivity plot is presented in Figure 5, where the sensitivity is defined as the percentage of the inductance change per µm of the sensing plate displacement at different gap sizes. The plot indicates that the sensitivity decreases exponentially with respect to the gap size. For example, a sensitivity of approximately 0.1 and 0.005 is achieved at 200 µm and 600 µm gap size, respectively. Therefore, it is critical to maintaining a small initial gap size to achieve high sensitivity.

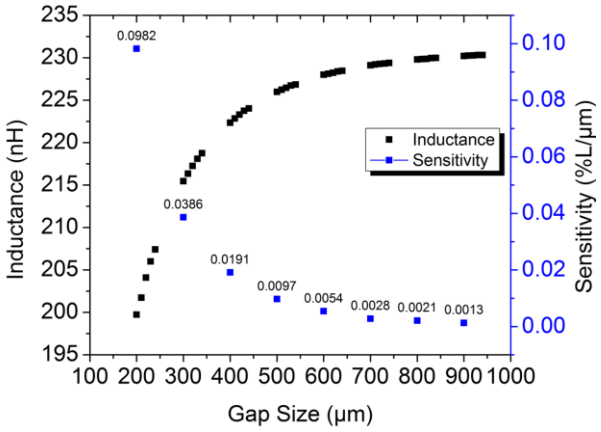

Fig. 5. Inductance value and sensitivity of the sensing coil vs. gap size.

B. *Sensing Coil Q-Factor Characterization*

The quality factor (Q-factor) of an inductor is a critical parameter for a low-power oscillator design employing the inductor as a frequency setting component as will be described in Section IV. The Q-factor of a packaged sensing coil, as depicted in Figure 4(b), is measured with and without the metallic sensing plate in 1xPBS solution. It should be noted that when the metallic sensing plate is employed, the gap size between the sensing coil and the plate is approximately 450 µm for the Q measurement. The measurement result indicates that the Q-factor exhibits about 10% reduction with the metallic sensing plate compared to without the plate across the frequency. For example, the sensing coil inductor achieves a Q-factor of approximately 22 and 20 at 40 MHz (oscillator frequency as will be described in the following section) with and without the metallic sensing plate, respectively. This is due to the reduced inductance and increased loss caused by the eddy current effect. The same experiment is conducted in air revealing a similar result as obtained in 1xPBS solution, which indicates that the 3D-printed package can effectively isolate the effect of 1xPBS solution from the sensing coil inductor.

IV. DC-Powered Prototype Sensing System Design And Packaging

A. *Tunnel Diode Oscillator-Based Inductive Sensor*

Figure 6 presents a tunnel diode oscillator-based inductive sensor design, where a commercial silicon tunnel diode (1N2928) is interfaced with an LC tank circuit consisting of a sensing coil (L_{Sense}) and a tuning capacitor (C_{Tune}) for the prototype system demonstration.

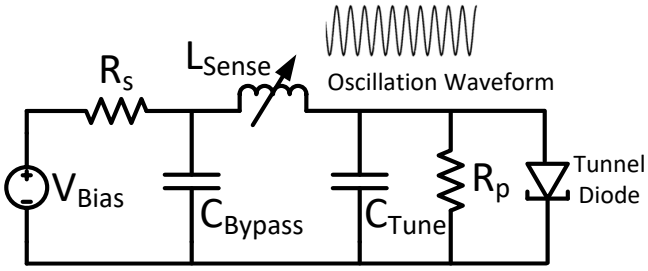

Fig. 6. Circuit schematic of DC-powered tunnel diode oscillator-based inductive sensor.

In addition, a bypass capacitor (C_{Bypass}) is employed to provide an AC ground for the sensing coil, a resistor (R_p) models the loss of the LC tank circuit, and V_{Bias} and R_s present the DC bias voltage for the tunnel diode and its associated source resistance, respectively. Under a proper oscillator design where the LC tank circuit loss is compensated by the negative resistance of the tunnel diode, an initial oscillation start-up can be produced with a resulting steady-state oscillation frequency expressed by Equation (1),

$$f = \frac{1}{2\pi\sqrt{L_{Sense}C_{Tune}}} \quad (1)$$

In the prototype design with a sensing coil inductance of approximately 200 nH, a tuning capacitor of 80 pF is selected to achieve a nominal oscillation frequency of around 40 MHz, which is close to the industrial, scientific, and medical radio band (ISM band). Furthermore, the LC tank circuit loss can be estimated around 1300 Ω at the oscillation frequency, which is mainly dominated by the loss associated with the sensing coil. As shown in Figure 7, the tunnel diode can achieve a negative resistance of approximately -1200 Ω with a bias voltage of 200 mV, which is sufficient to compensate the LC tank loss, thus ensuring a reliable oscillation start-up. It should be noted that the corresponding DC bias current of 210 µA results in a low power dissipation of only 42 µW, which is highly desirable for biomedical implant applications. Computer simulation further

reveals a steady-state oscillator amplitude of approximately 180 mV, responding to an RF power of -19 dBm, which is sufficient for signal telemetry for the proposed application.

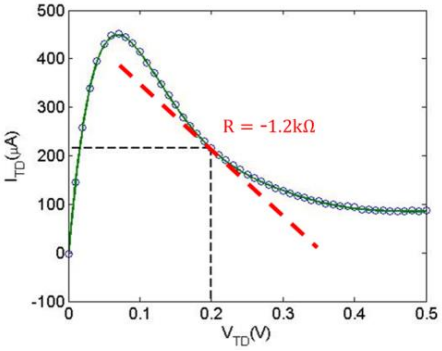

Fig. 7. Tunnel diode exhibiting negative resistance.

B. Fabrication of Glucose-Sensitive Hydrogel with Metallic Sensing Plate

Figure 8 presents the key processing steps of fabricating glucose-sensitive hydrogel with embedded metallic sensing plate. Glucose-sensitive hydrogel was synthesized using the optimum composition developed by Nguyen *et al*. [16, 21], which was composed of 3-(acrylamido)phenylboronic acid, acrylamide, N-[3-(dimethylamino)propyl]methacrylamide, N,N'-methylenebisacrylamide and (3-acrylamidoproply) trimethylammonium chloride. Details of preparation procedure of pre-gel mixture are described in [16, 21]. At this stage, a 3 mm x 3 mm corrosion-resistant aluminum plate with a thickness of approximately 80 μm, serving as a metallic sensing plate, was coated with a 10 μm-thick Parylene-C, followed by surface modification with vinyl group, which can achieve an improved bonding with the pre-gel mixture. The metallic sensing plate was then placed at the bottom of a PDMS mold exhibiting a height of 400 μm, followed by dispensing the pre-gel mixture with a predefined volume into the mold, as depicted in Figure 8. The mold was then covered by a 200 μm-thick GelBond® film. After the polymerization was completed, the polymerized film was then peeled away from the mold to obtain a glucose-sensitive hydrogel sample with the metallic sensing plate adhered on the top of the film as shown in Figure 8.

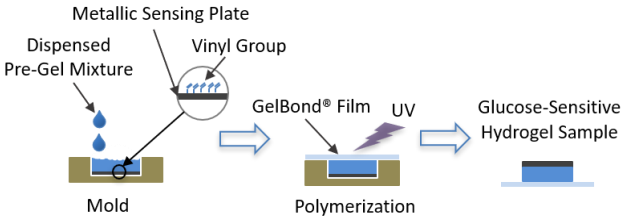

Fig. 8. Fabrication of glucose-sensitive hydrogel with metallic sensing plate

C. Prototype Sensor Package and Test Setup

Figure 9 depicts the prototype tunnel diode oscillator-based glucose sensor packaging and test setup, where the oscillator is assembled on an 8 mm-diameter PCB and is placed in a 10 mm-diameter 3D-printed cylindrical sensor package exhibiting a height of approximately 7 mm. The oscillator is powered by a DC power supply. The package is then filled with PDMS to seal the electronics followed by a 10 μm-thick Parylene C coating, serving as a biocompatible as well as a moisture-resistant layer. Ultimately, a fused glass package can be considered in the future to further enhance robustness. A fabricated 3 mm x 3mm x 400 μm glucose-sensitive hydrogel sample is adhered onto a 3D-printed adjustable platform by using Loctite 4011 medical device adhesive, which is further assembled onto the 3D-printed sensor package via three M2 screws. The gap size between the metallic sensing plate and the bottom of the sensor package can be adjusted to approximately 450 μm. The final gap size can be visualized and estimated by using an optical microscope (Keyence VHX-5000) as will be presented in Figure 10.

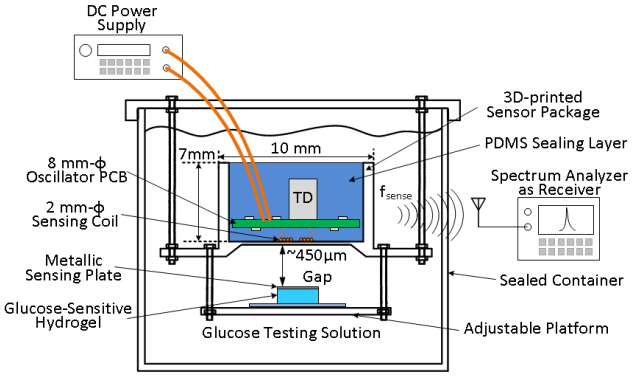

Fig. 9. Test setup for DC-powered oscillator-based glucose sensor.

The package is then placed into a sealed container with a controlled glucose concentration for *in-vitro* system characterization. A spectral analyzer is placed in proximity to receive wireless signals transmitted from the sensor. Figure 10 presents photos of the step-by-step sensor packaging sequence and test setup.

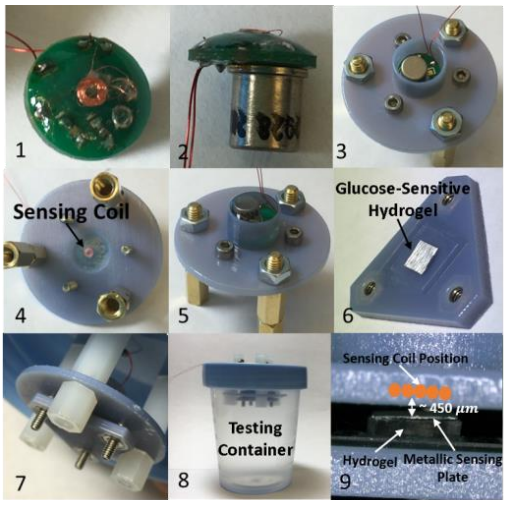

Fig. 10. (1) Oscillator PCB assembly; (2) Side view of the oscillator PCB; (3) Placing the oscillator PCB into a 3D-printed sensor package; (4) Bottom view of the packaged sensor showing the 2mm-ϕ sensing coil; (5) Top view of the packaged sensor sealed by PDMS; (6) Glucose-sensitive hydrogel embedding a metallic sensing plate on an adjustable platform; (7) Adjustable platform assembled onto the 3D-printed sensor package via screws; (8) Fully assembled sensor in a sealed testing container with a controlled glucose concentration; (9) Microscope photo showing the gap size between the metallic sensing plate and the sensing coil, where the position of the sensing coil is depicted for illustration purpose.

D. Glucose Measurement Results

A preliminary *in vitro* glucose test was performed under room temperature using the test setup depicted in Figure 9. The packaged sensor was first immersed in a solution with a 4 mM glucose concentration to reach a steady stage before the testing. Figure 11 presents a typical received power spectrum from the oscillator over a 4 cm telemetry distance. The received signal exhibits -78 dBm RF power around 38 MHz, which is close to the designed ISM band.

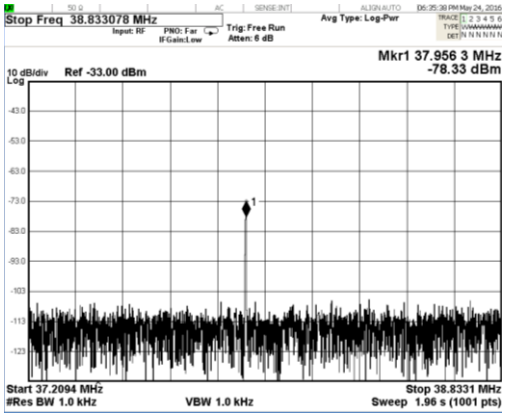

Fig. 11. Received oscillator spectrum.

The glucose concentration was then dropped to 0 mM and kept unchanged for 3 days to investigate the hydrogel response time and long-term frequency stability of the oscillator. After the initial 3-day period, the glucose concentration was increased from 0 mM to 10 mM with a step of 2 mM every 24 hours. Figure 12 presents the measured response characteristics indicating a sensitivity of 20 kHz/mM and 8.5 kHz/mM for a glucose concentration below 2 mM and around 10 mM, respectively. A total frequency shift of 107 kHz is observed over a concentration range of 10 mM, and the corresponding hydrogel sample thickness reduction is estimated to be approximately 52 µm.

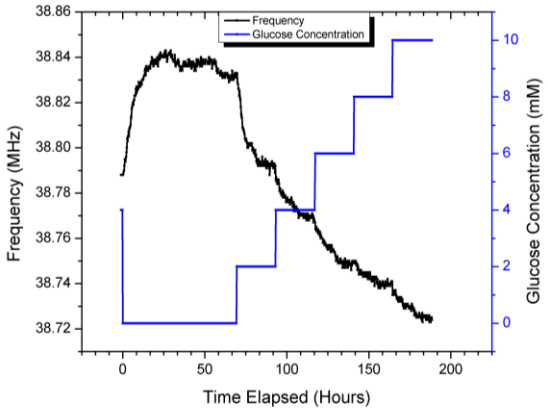

Fig. 12. DC-powered glucose sensor testing result.

The reduced sensitivity at higher concentration is likely due to the hydrogel saturation at higher glucose concentration and an increased gap size due to the hydrogel shrinking. It should be noted that the overall system sensitivity is proportional to the thickness of the hydrogel, which is 400 µm in the prototype design. A thicker hydrogel can be considered in the future to further enhance the sensitivity. The prototype oscillator exhibits a long-term frequency drift, likely caused by the ambient temperature variation, which can potentially limit the system sensing accuracy. As shown in Figure 12, the oscillator exhibits an approximately 5 kHz drift per day during the 2nd and the 3rd day when the glucose concentration was held unchanged. The frequency drift will result in a sensing accuracy of 0.2 mM at lower concentration and 0.6 mM at higher concentration. The measurement data also reveals a frequency fluctuation on the order of a few kHz, which is likely caused by the DC power supply voltage fluctuation. It is also observed that the response time of the hydrogel sample employed in this test is approximately 20 hours, which is long for practical glucose sensing applications. A substantially shortened response time can be achieved by employing a different hydrogel geometry, which will be described in the following Section V.

V. RF-Powered Glucose Sensor

A. RF-Powered Tunnel-Diode Oscillator

Figure 13 presents an RF-powered tunnel diode oscillator-based inductive sensor architecture for glucose sensing application. The overall system consists of a pair of tuned LC tanks for wireless RF power transfer, a Schottky diode half-wave rectifier, a voltage regulator, and a tunnel diode oscillator. The Schottky diode exhibits a forward voltage drop of approximately 200mV, critical for minimizing power loss. The voltage regulator is configured to output a stable 200mV DC bias voltage for the tunnel diode; hence, ensuring a stable oscillation frequency. The regulator internally consumes 70 µA bias current at 1.2V. With an output current of 210 µA delivered to the tunnel diode, an equivalent AC load resistance, R_{load}, of 2.56 kΩ is presented to the L_2C_2 tank circuit.

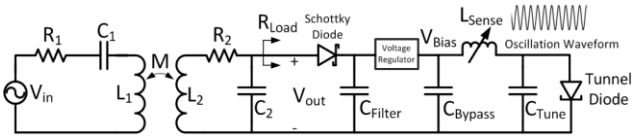

Fig. 13. RF-powered tunnel diode oscillator-based inductive sensor for glucose sensing.

It should be noted that multi-coils-based RF powering systems have been demonstrated to achieve an extended coupling distance [22, 23]. However, multiple implantable coils represent a significant challenge and practical inconvenience for biomedical implantable applications. Therefore, a two-coils-based architecture is selected for the prototype system design. It can be shown that the voltage gain and AC power transfer efficiency can be expressed in Equations (2) and (3), respectively,

$$A_v \approx kQ_1Q_2\sqrt{\frac{L_2}{L_1}}\frac{1}{1+\beta} \tag{2}$$

$$\eta = \frac{k^2Q_1Q_2\beta}{(1+\beta)^2} \tag{3}$$

where $\beta = \frac{(\omega L_2)^2}{R_{load}\,R_2}$ [24]. In the prototype design, a 5.5 cm-diameter 5-turn external coil exhibiting an inductance value of 3 µH is employed as the RF power transmitting coil of L_1, and a 0.9 cm-diameter 20-turn coil exhibiting an inductance

value of 6.5 μH is used as the RF power receiving coil of L_2. The size of the RF power transmitting coil is selected to be large enough to enable a deep powering distance while maintaining a reasonable dimension for typical hand-held and wearable devices. The size of the RF power receiving coil is chosen to be similar to the size of the prototype sensor package. Once the geometry of the coils and the RF powering depth are determined, the voltage gain (A_v) and AC power transfer efficiency (η) are only depended on the operating frequency. Since both the voltage gain and efficiency are important in this design, the optimization approach focuses on finding an RF powering frequency that maximizes the product of both parameters. As depicted in Figure 14, a design figure of merit (FOM), $A_v\eta/k^3$, is plotted against frequency. It should be noted that the coupling factor, k, is independent of frequency and is only depended on the coils dimension and effective distance in between. An optimal operating frequency in this design is found to be around 5MHz, where $A_v\eta/k^3$ is maximized. Consequently, with an RF powering distance of 2 cm, L_1 and L_2 being coaxially aligned, and a coupling factor of 0.013, a voltage gain of 24 and an AC power transfer efficiency of 14 % can be achieved. The prototype design, therefore, employs an RF voltage source, V_{in}, with an amplitude of 60 mV to develop a voltage swing exhibiting an amplitude of 1.4V in front of the Schottky diode to achieve a DC voltage of 1.2V to energize the voltage regulator, which furthers powers the oscillator. With a series resistance, R_1, of 0.65Ω, a total RF power of 2.77 mW is developed into the external LC tank consisting of L_1 and C_1. Variations in coils distance, offset and tilting angle will result in a certain performance alteration. However, the optimal frequency remains relatively constant. It should also be noted that the oscillator is designed to avoid frequency pulling due to the RF powering signal.

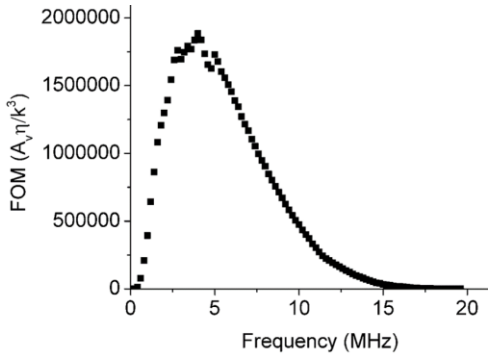

Fig. 14. RF powering design FOM versus frequency.

B. Pillar-Based Hydrogel Sensor Structure

As described in Section IV, the prototype 3 mm x 3 mm x 400 μm hydrogel slab exhibits a long response time under room temperature. It is known that hydrogel response time is proportional to the diffusion rate of glucose into the hydrogel, which is depended on the hydrogel surface-to-volume ratio and environment temperature. For the prototype hydrogel slab, both top and bottom surfaces are covered by the metallic sensing plate and Gelbond® film, respectively, thus substantially limiting the surface to volume ratio to approximately 1.3/mm. To increase the surface to volume ratio, a three-pillar-based hydrogel sensor structure is constructed as shown in Figure 15, where a metallic sensing plate is supported by three cylindrical pillars instead of a solid slab. The three pillars are chosen for structural stability. The hydrogel pillars are first formed by using a method similar to what is illustrated in Section V. The pillars are then adhered onto a GelBond® film followed by attaching the metallic sensing plate on top by using Loctite 4011 medical device adhesive. The dimension of each pillar is 1.3 mm in diameter and 1.5 mm in height with a spacing of approximately 1 mm among them, thus achieving an enhanced surface to volume ratio of around 3/mm.

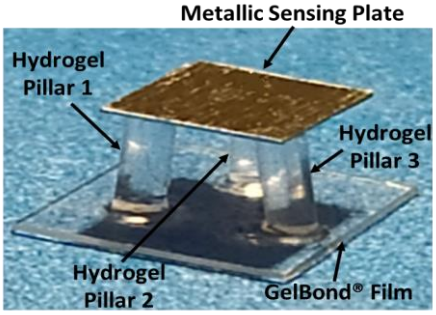

Fig. 15. Photo of a fabricated three-pillar-based hydrogel sensor structure.

C. RF-Powered Glucose Sensor Test Setup and Measurement Results

Figure 16 presents the RF-powered glucose sensor test setup, which shares a similar packaging scheme as the DC-powered sensor presented in the previous section. The powering distance between the RF power transmitting coil positioned on top of the testing apparatus and the RF power receiving coil packaged inside the sensor package is approximately 2 cm. It should be noted that the initial gap size between the metallic sensing plate and the sensing coil, which is encapsulated at the bottom of the sensor package, is adjusted to be around 450 μm.

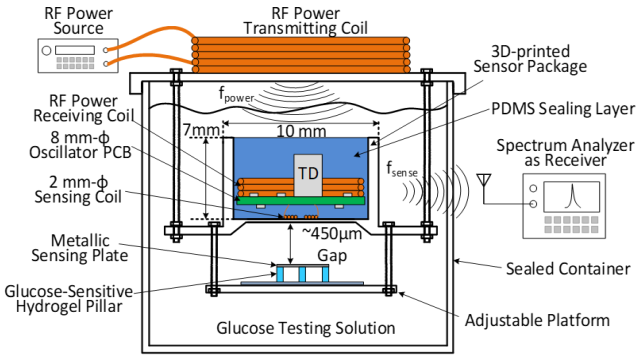

Fig. 16. RF-powered glucose sensor test setup.

The glucose testing results of the RF-powered glucose sensor is presented in Figure 17, where the glucose concentration was first increased from 0 mM to 10 mM with an incremental step of 2 mM, followed by an abrupt decrease down to 0 mM. Compared to the 3 mm x 3 mm x 400 μm hydrogel slab-based sensor, the pillar-based hydrogel sensor exhibits a much faster response time of approximately 2 hours. The hydrogel response time is defined as the time interval from a step glucose change to a point when the oscillator frequency reaches its steady-state, where an observable frequency change is within the oscillator inherent frequency fluctuation on the order of 3 kHz peak-to-peak. Besides, the sensor exhibits different sensitivities within different glucose ranges, similar to the hydrogel

slab-based sensor described in Section IV. In particular, the highest sensitivity of approximately 60 kHz/mM is observed at low glucose concentration from 0 mM to 2 mM, and the lowest sensitivity of about 10 kHz/mM is obtained from 8 mM to 10 mM glucose concentration, thus corresponding to a sensing resolution of 0.05 mM and 0.3 mM, respectively. A total gap change of approximately 144 μm is estimated between the metallic sensing plate and the sensing coil when the glucose concentration is increased from 0 mM to 10 mM. The measurement data further reveals that the pillar-based glucose sensor exhibits a reversible glucose-sensing capability with approximately 25% less frequency change when the glucose concentration decreases from 10 mM to 0 mM. It is speculated that this frequency discrepancy between the upward and downward glucose change is likely due to hydrogel hysteresis caused by the mechanical loading of the metallic sensing plate on top of the hydrogel pillars. Due to the hysteresis, the initial gap size of the second glucose testing cycle is larger than that of the first cycle. Therefore, the sensor exhibits a reduced frequency change of approximately 80% of the frequency change from the first testing cycle. A similar hysteresis behavior was observed when employing a pressure sensor monitoring approach [25]. Furthermore, it also should be noted that compared to Figure 12, the RF-powered sensor achieves a much cleaner frequency plot due to the elimination of long power supply wires.

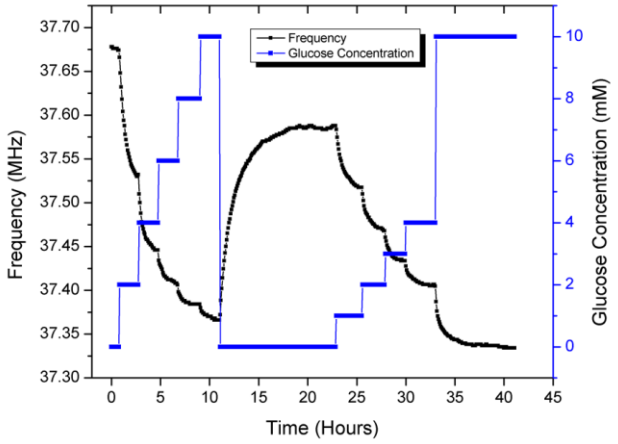

Fig. 17. RF-powered pillar-based glucose sensor test results.

Besides characterizing the sensor response to the glucose concentration change, it is critical to investigate the long-term oscillator frequency stability for implantable applications.
The sensor was powered on wirelessly and submersed in a testing container containing 1xPBS solution with 4 mM glucose concentration over 25 hours. The oscillator frequency and ambient temperature were recorded simultaneously during the test. As shown in Figure 18, the oscillator exhibits a temperature-dependent frequency fluctuation. From this test, a peak-to-peak frequency drift of approximately 10 kHz is observed with a temperature variation around 1.6 °C. This temperature-dependent behavior can ultimately limit the system sensing resolution. It is, therefore, highly desirable to incorporate a temperature sensor for calibration purpose in future system design.

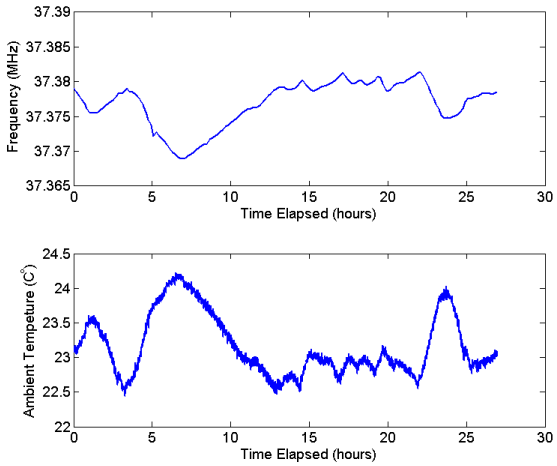

Fig. 18. Temperature-dependent oscillator frequency drift.

VI. Discussion

The performance of the prototype implantable hydrogel-based glucose sensor is compared to that of other published continuous glucose monitoring devices as presented in Table I. Continuous glucose sensors are mainly composed of two categories: (1) long-term implantable glucose sensors and (2) short-term glucose sensors. Compared to the long-term implantable glucose sensors, which employ fluorescent and hydrogel-based capacitive sensing principles [11, 12, 26], the prototype system achieves the lowest power dissipation with a comparable sensing resolution enabled by the inductive sensing scheme and low-power tunnel diode oscillator. The sensor is MRI compatible due to the use of an air-core RF power receiving coil, thanks to the low system power dissipation. Furthermore, the robust package encapsulating all electronic components ensures hermeticity, which is highly desirable for long-term implantable applications. The short-term glucose sensors are based on an electrochemical sensing scheme [27-29]. While these sensors consume a reduced power due to their sensing mechanism, these devices, however, rely on non-hermetic packages, which severely limit the sensors lifetime.

LC resonator-based passive sensing and telemetry principles have been employed to implement hydrogel-based glucose sensors [30, 31] and other types of devices for *in-vivo* restenosis and occlusion detection [32] and intraocular pressure sensing [33]. While a passive sensing and telemetry scheme can simplify the overall sensor system design, this approach, however, suffers from a degraded sensing resolution due to a limited quality factor of the LC resonator and external frequency-scanning signal quality in terms of its frequency interval and resolution [34]. Furthermore, miniature implant form factor calls for a small inductor dimension, which in turn substantially limits the telemetry distance. On the other hand, an active LC resonator-based sensing and telemetry implementation can improve sensing resolution and enhance telemetry distance, which is desirable for practical implantable applications.

TABLE I
PERFORMANCE COMPARISON TABLE FOR CONTINUOUS GLUCOSE SENSORS.

	Long-term Implantable Glucose Sensors				Short-term Glucose Sensors		
	This work	[11]	[12]	[26]	[27]	[28]	[29]
Power	336 μW	3.35 mW	3 mW	943 μW	50 μW	3 μW	200 μW
Sensing Resolution	0.05mM (0-2mM) 0.3mM (8-10mM)	0.06mM	0.3 mM	0.1mM	0.2mM	39.6nA/mM	0.1mM
Sensing Principle	GSH-Inductive	Fluorescent	Fluorescent	GSH Capacitive	Electrochemical	Electrochemical	Electrochemical
Signal Transmission	Active Wireless	Passive Wireless	Wired	Active Wireless	Passive Wireless	Passive Wireless	Passive Wireless
RF Power Receiving Coil Core	Air Core	Ferrite Core	NA	NA	Ferrite Core	Air Core	Air Core
MRI Compatibility	Yes	Yes	NA	NA	No	Yes	Yes

TABLE II
WIRELESS POWER TRANSFER COMPARISON TABLE FOR BIOMEDICAL IMPLANTS.

	This work	[11]	[22]	[24]	[27]	[35]	[36]
Power Transfer Efficiency	14%	72%	21%	3% at 4 cm 7×10^{-5} at 20 cm	0.4%	10%	3.8×10^{-5}
Implantable Power Receiving Coil Size	10 mm-Φ Spiral	2 mm-Φ x 15.7mm Solenoid	2 mm-Φ Spiral	7 mm x 17 mm Spiral	1.2 mm-Φ x 5 mm Solenoid	6 mm-Φ Spiral	1. 4 mm x 1.4 mm Spiral
Implantable Power Receiving Coil Core	Air Core	Ferrite Core	Air Core with Intermediate Coil	Ferrite Core	Ferrite Core	Air Core	Air Core
Operating Frequency	5 MHz	13.56 MHz	60 MHz	3 MHz	13.56 MHz	8 MHz	900 MHz
Powering Distance	2 cm	2 cm	5 mm	4 cm to 20 cm	2.5 cm	1 cm	1 cm

Wireless power transfer techniques based on an inductive coupling principle have been applied for various biomedical implant applications [11, 22, 24, 27, 35, 36]. Table II summarizes the wireless power transfer efficiency comparing the prototype system to a number of published works. It should be noted that the efficiency strongly depends on the implantable power receiving coil dimension, core material, wire dimension and conductivity, operating frequency, as well as distance and orientation with respect to an external power transmitting coil.

VII. Conclusion and Future Work

This paper presents a wireless inductive sensing technology with a robust packaging scheme for future implantable hydrogel-based glucose monitoring applications. The wireless inductive sensing scheme is highly desirable for interfacing with a glucose-sensitive hydrogel serving as a sensing element. This approach allows the sensing electronics to be fully encapsulated in a 3D-printed hermetic package without the need of a deflectable sensing membrane, thus greatly improving the package robustness for long-term implantable applications. A low-power tunnel diode oscillator is designed to wirelessly transmit the glucose information through frequency modulation. The oscillator can be energized by RF powering to realize complete standalone wireless and battery-less operation. A prototype sensing system was characterized *in vitro* and demonstrated a sensing resolution of 0.05 mM and 0.3 mM

within a glucose range from 0 mM to 2 mM and 8 mM to 10 mM, respectively, limited by the oscillator frequency drift and fluctuation. Furthermore, a hydrogel pillar-based design achieves an enhanced surface to volume ratio, thus substantially shortening the system response time compared to a hydrogel slab-based design. It is anticipated that an improved hydrogel response time can be obtained by employing porous hydrogel material as well as designing hydrogel structures exhibiting a large surface to volume ratio. A temperature sensor will be co-designed in the future to provide temperature calibration, which is important for a practical implant application. A low-power ASIC design will be implemented to achieve further system miniaturization.

Prashant Tathireddy has financial and business interest in Applied Biosensors, LLC that may be affected by the research reported in this paper.

REFERENCES

[1] S. K. Vashist, "Continuous Glucose Monitoring Systems: A Review", *Diagnostics*, 2013, vol. 3, pp.385-412.

[2] H. Yao, A. J. Shum, M. Cowan, I. Lähdesmäki, and B. A. Parviz, "A contact lens with embedded sensor for monitoring tear glucose level," *Biosensors and Bioelectronics*, vol. 26, pp. 3290-3296, 2011.

[3] H. Lee, C. Song, Y. S. Hong, M. S. Kim, H. R. Cho, T. Kang, et al., "Wearable/disposable sweat-based glucose monitoring device with multistage transdermal drug delivery module," *Science advances*, vol. 3, p. e1601314, 2017.

[4] W. Zhang, Y. Du, and M. L. Wang, "Noninvasive glucose monitoring using saliva nano-biosensor," *Sensing and Bio-Sensing Research*, vol. 4, pp. 23-29, 2015.

[5] B. Leboulanger, M. Fathi, R. H. Guy, and M. B. Delgado-Charro, "Reverse iontophoresis as a noninvasive tool for lithium monitoring and pharmacokinetic profiling," *Pharmaceutical research*, vol. 21, pp. 1214-1222, 2004.

[6] E.-J. Park, J. Werner, J. Beebe, S. Chan, and N. B. Smith, "Noninvasive ultrasonic glucose sensing with large pigs (~ 200 Pounds) using a lightweight cymbal transducer array and biosensors," *Journal of Diabetes Science and Technology*, vol. 3, pp. 517-523, 2009.

[7] O. Amir, D. Weinstein, S. Zilberman, M. Less, D. Perl-Treves, H. Primack, et al., "Continuous noninvasive glucose monitoring technology based on "occlusion spectroscopy"," *ed: SAGE Publications*, 2007.

[8] J. C. Pickup, F. Hussain, N. D. Evans, and N. Sachedina, "In vivo glucose monitoring: the clinical reality and the promise," *Biosensors and Bioelectronics*, vol. 20, pp. 1897-1902, 2005.

[9] J. C. Pickup, F. Hussain, N. D. Evans, O. J. Rolinski, and D. J. Birch, "Fluorescence-based glucose sensors," *Biosensors and Bioelectronics*, vol. 20, pp. 2555-2565, 2005.

[10] Y. J. Heo, H. Shibata, T. Okitsu, T. Kawanishi, and S. Takeuchi, "Long-term in vivo glucose monitoring using fluorescent hydrogel fibers," *Proceedings of the National Academy of Sciences*, vol. 108, pp. 13399-13403, 2011.

[11] A. DeHennis, S. Getzlaff, D. Grice, and M. Mailand, "An NFC-enabled CMOS IC for a wireless fully implantable glucose sensor," *IEEE journal of biomedical and health informatics*, vol. 20, pp. 18-28, 2015.

[12] T. Tokuda, T. Kawamura, K. Masuda, T. Hirai, H. Takehara, Y. Ohta, et al., "*In Vitro* Long-Term Performance Evaluation and Improvement in the Response Time of CMOS-Based Implantable Glucose Sensors," *IEEE Design & Test*, vol. 33, pp. 37-48, 2016.

[13] H. Shibata, Y. J. Heo, T. Okitsu, Y. Matsunaga, T. Kawanishi, and S. Takeuchi, "Injectable hydrogel microbeads for fluorescence-based *in vivo* continuous glucose monitoring," *Proceedings of the National Academy of Sciences*, vol. 107, pp. 17894-17898, 2010.

[14] Y. J. Heo, H. Shibata, T. Okitsu, T. Kawanishi, and S. Takeuchi, "Long-term *in vivo* glucose monitoring using fluorescent hydrogel fibers," *Proceedings of the National Academy of Sciences*, vol. 108, pp. 13399-13403, 2011.

[15] P.-H. Kuo, S.-S. Lu, J.-C. Kuo, Y.-J. Yang, T. Wang, Y.-L. Ho, et al., "A hydrogel-based implantable wireless CMOS glucose sensor SoC," *IEEE International Symposium on Circuits and Systems*, 2012, pp. 994-997.

[16] T. Nguyen, P. Tathireddy, J. Magda, "Continuous hydrogel-based glucose sensors with reduced pH interference and contact-free signal transduction," *IEEE Sensors Journal*, vol. 19, pp. 2330-2337, 2019.

[17] J. Park, S. Song, G. Chitnis, R. Siegel, and B. Ziaie, "A wireless chemical sensor using ferroparticles embedded hydrogel," in Solid-State Sensors, Actuators and Microsystems (TRANSDUCERS & EUROSENSORS XXVII), 2013 Transducers & Eurosensors XXVII: The 17th International Conference on, 2013, pp. 1735-1738.

[18] Y. Yu, T. Nguyen, P. Tathireddy, S. Roundy, and D. J. Young, "Wireless Hydrogel-Based Glucose Sensor for Future Implantable Applications (Invited)," *IEEE Sensors Conference*, Orlando, Florida, October 2016, pp. 1667-1669.

[19] E. Y. Chow, A. L. Chlebowski, S. Chakraborty, W. J. Chappell, and P. P. Irazoqui, "Fully wireless implantable cardiovascular pressure monitor integrated with a medical stent," *IEEE Transactions on Biomedical Engineering*, vol. 57, pp. 1487-1496, 2010.

[20] E. Y. Chow, Y. Ouyang, B. Beier, W. J. Chappell, and P. P. Irazoqui, "Evaluation of cardiovascular stents as antennas for implantable wireless applications," *IEEE Transactions on Microwave Theory and Techniques*, vol. 57, pp. 2523-2532, 2009.

[21] T. Nguyen, J. J. Magda, and P. Tathireddy, "Manipulation of the isoelectric point of polyampholytic smart hydrogels in order to increase the range and selectivity of continuous glucose sensors," *Sensors and Actuators B: Chemical*, vol. 255, pp. 1057-1063, 2018.

[22] Y. Jia, S. A. Mirbozorgi, B. Lee, W. Khan, F. Madi, A. Weber, et al., "A mm-sized free-floating wirelessly powered implantable optical stimulating system-on-a-chip," *IEEE International Solid-State Circuits Conference-(ISSCC)*, 2018, pp. 468-470.

[23] A. K. RamRakhyani and G. Lazzi, "On the design of efficient multi-coil telemetry system for biomedical implants," *IEEE Transactions on Biomedical Circuits and Systems*, vol. 7, pp. 11-23, 2013.

[24] D. J. Young, P. Cong, M. A. Suster, and M. Damaser, "Implantable wireless battery recharging system for bladder pressure chronic monitoring," *Lab on a Chip*, vol. 15, pp. 4338-4347, 2015.

[25] T. Nguyen, S. Cho, V. Bhola, S. Ko, R. Sharma, J. Magda, et al., "Sensor-array for continuous monitoring of biochemicals for bioprocess control," *Solid-State Sensors, Actuators and Microsystems (TRANSDUCERS)*,Transducers 18th International Conference on, 2015, pp. 1684-1687.

[26] Y.-J. Huang, T.-H. Tzeng, T.-W. Lin, C.-W. Huang, P.-W. Yen, P.-H. Kuo, et al., "A self-powered CMOS reconfigurable multi-sensor SoC for biomedical applications," *IEEE Journal of Solid-State Circuits*, vol. 49, pp. 851-866, 2014.

[27] Z. Xiao, X. Tan, X. Chen, S. Chen, Z. Zhang, H. Zhang, et al., "An implantable RFID sensor tag toward continuous glucose monitoring," *IEEE journal of biomedical and health informatics*, vol. 19, pp. 910-919, 2015.

[28] Y.-T. Liao, H. Yao, B. Parviz, and B. Otis, "A 3μW wirelessly powered CMOS glucose sensor for an active contact lens," *IEEE International Solid-State Circuits Conference*, 2011, pp. 38-40.

[29] M. M. Ahmadi and G. A. Jullien, "A wireless-implantable microsystem for continuous blood glucose monitoring," *IEEE Transactions on Biomedical Circuits and Systems,* vol. 3, pp. 169-180, 2009.

[30] M. Lei, A. Baldi, E. Nuxoll, R. A. Siegel, and B. Ziaie, "A hydrogel-based implantable micromachined transponder for wireless glucose measurement," *Diabetes Technology & Therapeutics*, vol. 8, pp. 112-122, 2006.

[31] M. Lei, A. Baldi, E. Nuxoll, R. A. Siegel, and B. Ziaie, "Hydrogel-based microsensors for wireless chemical monitoring," *Biomedical microdevices*, vol. 11, pp. 529-538, 2009.

[32] X. Chen, B. Assadsangabi, Y. Hsiang, and K. Takahata, "Enabling Angioplasty‐Ready "Smart" Stents to Detect In‐Stent Restenosis and Occlusion," *Advanced Science*, vol. 5, p. 1700560, 2018.

[33] P.-J. Chen, S. Saati, R. Varma, M. S. Humayun, and Y.-C. Tai, "Wireless intraocular pressure sensing using microfabricated minimally invasive flexible-coiled LC sensor implant," *Journal of Microelectromechanical Systems*, vol. 19, pp. 721-734, 2010.

[34] Q. Wei, Y. Wang, D. Chen, J. Chen, and J. Wang, "A novel method based on RF detection enabling wireless and passive LC sensing," *IEEE SENSORS, 2016 ,* pp. 1-3.

[35] B. D. Farnsworth, R. J. Triolo and D. J. Young, "Wireless Implantable EMG Sensing Microsystem," *IEEE Sensors Conference,* 2008, pp. 1245-1248.

[36] M. H. Nazari, M. Mujeeb-U-Rahman, and A. Scherer, "An implantable continuous glucose monitoring microsystem in 0.18 μm CMOS," *IEEE Symposium on VLSI Circuits*, 2014, pp. 1-2.